Journal of the Royal Statistical Society
SERIES C Applied Statistics

Appl. Statist. (2010)
59, *Part* 1, *pp.* 77–103

Fusing point and areal level space–time data with application to wet deposition

Sujit K. Sahu,

University of Southampton, UK

Alan E. Gelfand

Duke University, Durham, USA

and David M. Holland

Environmental Protection Agency, Research Triangle Park, USA

[Received July 2008. Revised April 2009]

Summary. Motivated by the problem of predicting chemical deposition in eastern USA at weekly, seasonal and annual scales, the paper develops a framework for joint modelling of point- and grid-referenced spatiotemporal data in this context. The hierarchical model proposed can provide accurate spatial interpolation and temporal aggregation by combining information from observed point-referenced monitoring data and gridded output from a numerical simulation model known as the 'community multi-scale air quality model'. The technique avoids the change-of-support problem which arises in other hierarchical models for data fusion settings to combine point- and grid-referenced data. The hierarchical space–time model is fitted to weekly wet sulphate and nitrate deposition data over eastern USA. The model is validated with set-aside data from a number of monitoring sites. Predictive Bayesian methods are developed and illustrated for inference on aggregated summaries such as quarterly and annual sulphate and nitrate deposition maps. The highest wet sulphate deposition occurs near major emissions sources such as fossil-fuelled power plants whereas lower values occur near background monitoring sites.

Keywords: Change-of-support problem; Hierarchical model; Markov chain Monte Carlo sampling; Measurement error model; Spatial interpolation; Stochastic integrals

1. Introduction

The combustion of fossil fuel produces a wide variety of chemicals, including such gases as sulphur dioxide and nitrogen oxides. These gases are emitted to the air, transformed to acidic compounds and then returned to the Earth. Most of the acid deposition in eastern USA can be attributed to the release of sulphur dioxide and nitrogen oxides from large fossil-fuelled power plants. When delivered by precipitation, such as rain, snow or fog, the process is called wet sulphate and nitrate deposition. Wet deposition is responsible for damage to lakes, forests and streams.

The primary objective of this study is to develop a high resolution model for wet chemical deposition that offers better inference than is currently possible by using just National Atmos-

Address for correspondence: Sujit K. Sahu, School of Mathematics, University of Southampton, Highfield, Southampton, SO17 1BJ, UK.
E-mail: S.K.Sahu@soton.ac.uk

 0035–9254/10/59077

pheric Deposition Program (NADP) (`nadp.sws.uiuc.edu`) wet deposition measurements and classical interpolation techniques. The model proposed uses deposition and precipitation data from NADP monitoring sites and output from a computer simulation model that is known as the 'community multi-scale air quality (CMAQ) model' (`epa.gov/asmdnerl/CMAQ`) on a 12 km $\times$ 12 km grid. The CMAQ model uses variables, such as power station emission volumes, meteorological information and land use, to predict average levels of deposition. However, it is well known that these predictions are biased; the monitoring data provide more accurate deposition information. The mismatch in the spatial domains for the point- and grid-referenced computer output is often alluded to as the 'change-of-support problem' and creates challenges in modelling and model fitting; see later for more details. Combining information from disparate sources is a relatively new activity in modelling air and deposition data, but it is fundamental to providing improved information for environmental decisions and enabling greater understanding of the processes that underlie deposition.

The contribution of this paper is the development of a joint model by combining a conditionally auto-regressive (CAR) model for the gridded CMAQ data and a space–time process model for observed point level data. Model components are linked by using latent space–time processes in a Bayesian hierarchical modelling set-up. All predictive inference is performed by using the point level model. A key feature of our strategy is avoidance of stochastic integration of the observed point level monitoring process to a grid level process.

More precisely, the average deposition level in a grid cell A_j at time t, which is denoted by $Z(A_j, t)$, need not be the level that is observed at any particular site $\mathbf{s}_i$ in A_j, which is denoted by $Z(\mathbf{s}_i, t)$. The change-of-support problem in this context addresses converting the point level $Z(\mathbf{s}_i, t)$ to the grid level $Z(A_j, t)$ through the stochastic integral,

$$Z(A_j, t) = \frac{1}{|A_j|} \int_{A_j} Z(\mathbf{s}, t)\, \mathrm{d}\mathbf{s}, \tag{1}$$

where $|A_j|$ denote the area of the grid cell A_j. Fusion modelling, working with *block averaging* as in equation (1), has been considered by, for example, Fuentes and Raftery (2005).

Our approach introduces a latent point level atmospheric process which is centred, in the form of a measurement error model (MEM), on a grid-cell-based latent atmospheric process. The latent processes are introduced to capture point masses at zero with regard to deposition whereas the MEM circumvents the stochastic integration. In particular, the point level observed data represent 'ground truth' whereas gridded CMAQ output is expected to be biased. As a result, the MEM enables calibration of the CMAQ model. The opposite problem of disaggregation, i.e. converting the grid level computer output denoted by $Z(A_j, t)$ to point level outputs $Z(\mathbf{s}_i, t)$, is not required. The only assumption is that $Z(A_j, t)$ is a reasonable surrogate for $Z(\mathbf{s}_i, t)$ if the site $\mathbf{s}_i$ is within the grid cell A_j. (This is confirmed by empirical evidence; see the discussion about Fig. 5 in Section 2.)

The amount of wet deposition is directly related to precipitation—there can be no deposition without precipitation. Hence, accurate predictions here require utilization of precipitation information. Note that both the precipitation and the deposition data have atomic distributions, i.e. they are continuous random variables with positive mass at zero. Our proposal is to build a model for deposition based on precipitation which can handle these atoms. We introduce a conceptual latent space–time atmospheric process which drives both precipitation and deposition as assumed in the mercury deposition modelling of Rappold *et al.* (2008). However, Rappold *et al.* (2008) did not address the fusion problem with modelled output. Rather, they used a point level joint process model, specified conditionally for the atmospheric, precipitation and

deposition processes. We incorporate a huge amount of CMAQ numerical model output data at 12-km-grid scale.

The wet deposition model is applied separately to the wet sulphate and wet nitrate deposition. There is high positive correlation between the compounds because of their dependence on precipitation but our interest here is to predict the sulphate and nitrate depositions separately. The model is fitted at point level spatial resolution and weekly temporal resolution, enabling spatial interpolation and temporal prediction of deposition as well as aggregation in space or time to facilitate seeing patterns and trends in deposition.

Our fully model-based approach removes many of the shortcomings of inverse distance weighting (IDW), which was used by the NADP to predict annual spatial patterns of wet deposition; see `nadp.sws.uiuc.edu/isopleths/annualmaps.asp`. The IDW method interpolates a deposition value at a new site by taking weighted means of depositions at data sites; the weights are inversely proportional to the square of the distance between the interpolation site and the data sites. Hence, these interpolations are most accurate near the data sites. However, IDW has serious limitations:

(a) it cannot accommodate covariate information;
(b) handling of missing observations by simple averaging of available observations is *ad hoc* and fails to take account of variability in these observations;
(c) it is not possible to associate any sort of uncertainty with estimated quarterly or annual totals, i.e. to provide uncertainty maps for the region;
(d) it does not recognize the problem of point mass at 0 (ordinary kriging suffers similar prob-

Fig. 1. Map of the study region: ●, modelled NADP sites; A–H, the eight validation sites

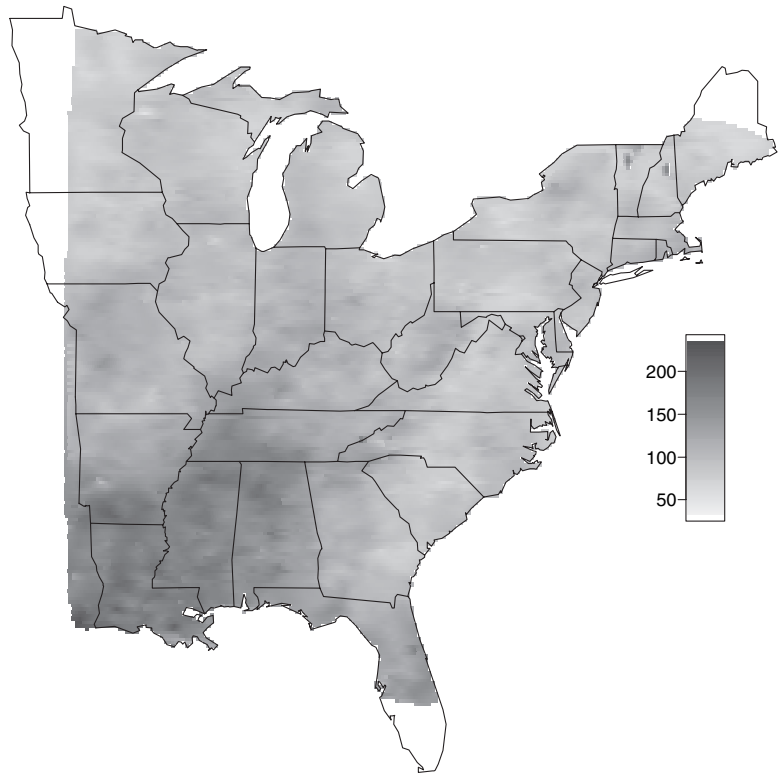

Fig. 2. Map of total annual precipitation in 2001

lems and, by ignoring uncertainty in model parameters, tends to underestimate predictive variability);

(e) modelling at an annual scale is possible but sacrifices process understanding that is available at a weekly resolution.

In recent years there has been a surge of interest in developing methods for modelling space–time data. Hierarchical Bayesian approaches for spatial prediction of air pollution have been developed; see, for example, Brown *et al.* (1994), Huerta *et al.* (2004), Le and Zidek (1992), Sahu and Mardia (2005), Sahu *et al.* (2006, 2007, 2009) and Wikle (2003). However, there are only a handful of references which have discussed models for wet deposition. Haas (1990a, b, 1995, 1996) used statistical methods including moving window regression, kriging and co-kriging and spatiotemporal modelling to study various aspects of depositions. Oehlert (1993) used a spatiotemporal model to estimate trend in annual sulphate depositions. Bilonick (1985) used classical geostatistical methods to model the space–time covariance structure of wet sulphate deposition. Grimm and Lynch (2004) developed a high resolution model for wet sulphate and nitrate deposition using precipitation and many topographic variables observed over a dense grid. Rappold *et al.* (2008) modelled wet mercury deposition data. Fuentes and Raftery (2005) offered the only fusion of data work in this area. However, their analysis is not dynamic and fitting their model with a large number of grid cells becomes computationally infeasible, as we clarify below.

The remainder of this paper is organized as follows. In Section 2 we describe the available data. Modelling developments are presented in Section 3. Prediction details are discussed in

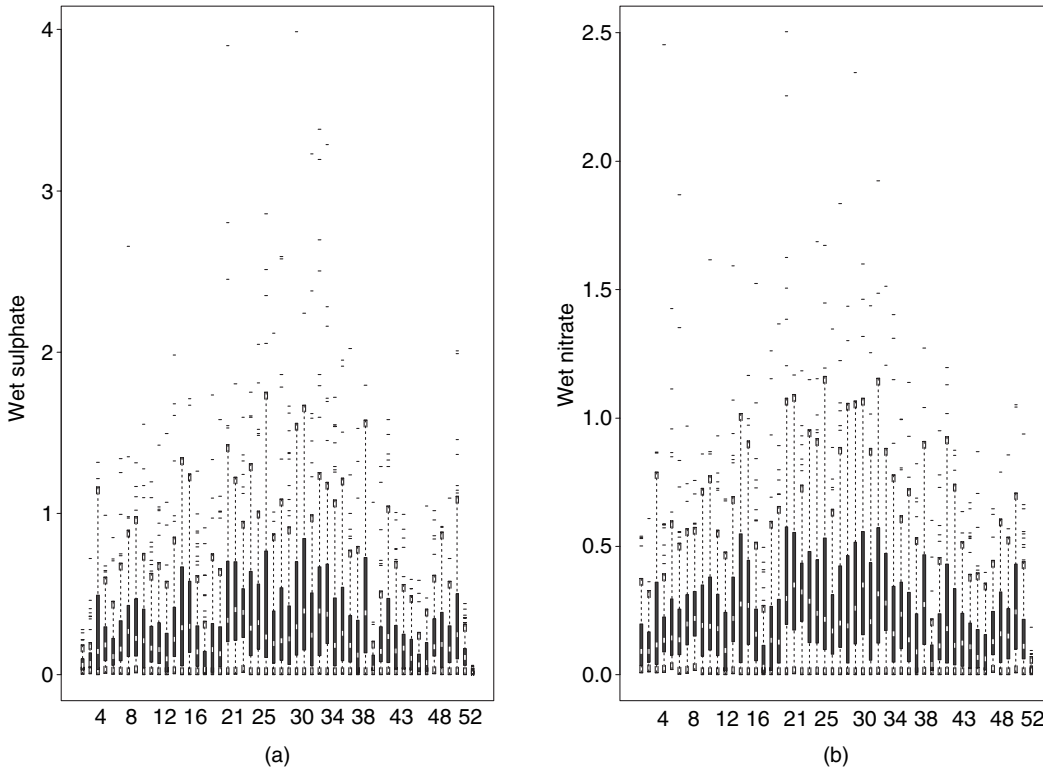

Fig. 3. Box plots of weekly depositions: (a) wet sulphate; (b) wet nitrate

Section 4. Section 5 provides the modelling results and analyses. A few summary remarks are provided in Section 6 and Appendix A contains the computational details for Gibbs sampling.

The data that are analysed in the paper can be obtained from

`http://www.blackwellpublishing.com/rss`

2. Exploratory analysis

We have weekly deposition and precipitation data for the 52 weeks in the year 2001 from 128 sites in eastern USA; see Fig. 1 for their locations. We use data from $n = 120$ sites for model estimation and prediction and the data for the remaining eight sites are used for validation. The validation sites are marked as A–H in Fig. 1 and have been chosen on the basis of several considerations. The eight sites are spread across the study region without forming clusters. The validation sites are some distance away from nearest data sites; in fact the distance between a validation site and its nearest data site ranges from 40 km to 186 km. More specifically, sites A and D are chosen because they fall in a high precipitation area (see Fig. 2 for the annual precipitation map). Site H is chosen because it is in an area where annual deposition is higher than average. There are nine missing observations (out of a total of $416 = 8 \times 52$) in the validation data set, most of which are for week 52, the end of the year holiday period in the USA.

There are 6240 ($= 120 \times 52$) observations in our modelling data set in total. For precipitation and deposition, 536 ($\approx 8.6\%$) of these were missing. The precipitation and deposition values in 507 location–week combinations (out of the remaining 5704) were 0. The deposition values in additional 119 location–week combinations were also recorded as missing. Hence, there are 655

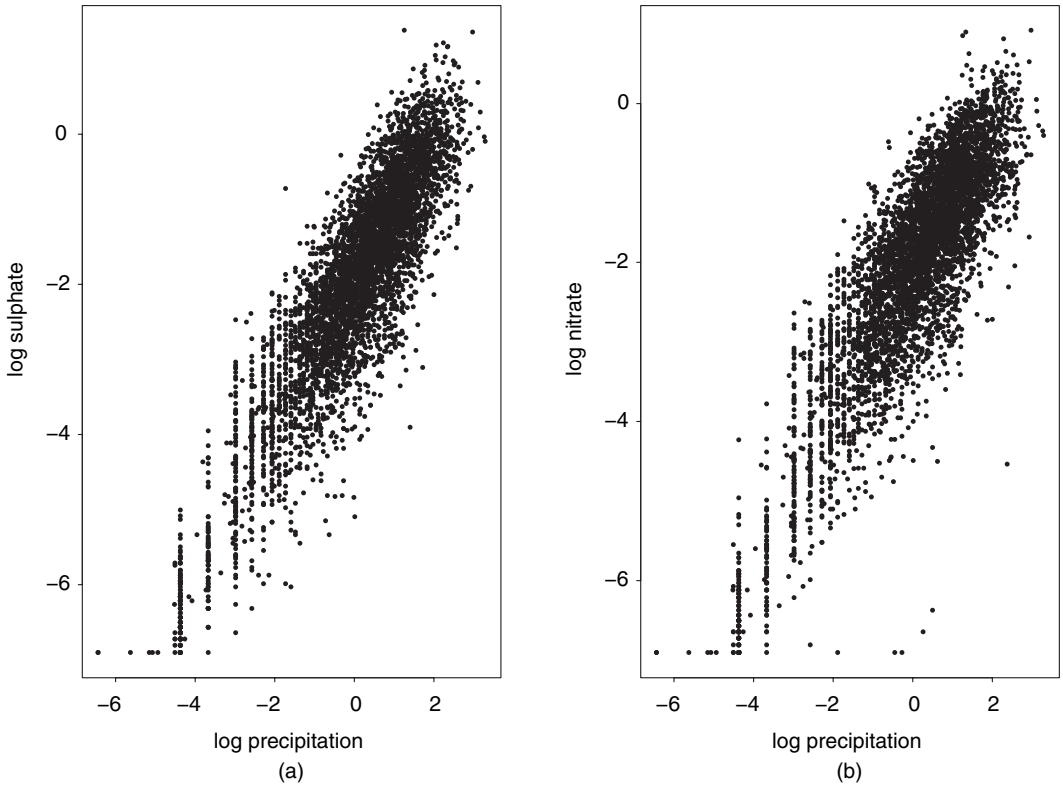

Fig. 4. Deposition against precipitation on the log-scale: (a) wet sulphate; (b) wet nitrate

location–week combinations ($\approx 10.5\%$) where deposition values were missing. We note that at each location and week combination either both the two types of deposition values are positive or both are 0, i.e. one cannot be 0 without the other being 0 as well. We also note that positive precipitation necessarily implies positive deposition (which sometimes can be very small).

The boxplots of the weekly sulphate and nitrate depositions in units of kilograms per hectare are plotted in Fig. 3. The labels on the horizontal axes are the last week of the months. Fig. 3 confirms the well-known fact that depositions levels are higher on average for the wetter spring and summer months than the dryer winter months; see for example, Brook *et al.* (1995). Strong linear relationships between deposition and precipitation on the log-scale are seen in Fig. 4.

We model weekly CMAQ output from $J = 33\,390$ grid cells covering our study region yielding 1 736 280 modelled values for the year. There is some evidence of a linear relationship on the log-scale between observed deposition and CMAQ model output for the cell containing the observation location, especially for higher values; see Fig. 5. The association between the two is degraded towards the lower end of the scale owing to zero values which have been replaced by a small positive number to avoid taking the logarithm of 0. This is done for data presentation purposes only.

For spatial prediction we have weekly precipitation data from 2827 predictive sites covering our study region. A map of the annual total precipitation (in centimetres) is provided in Fig. 2. Areas in the south-west corner of the map received more precipitation than others. However, in the model fitting we used only the precipitation data from the 120 NADP monitoring sites where we have deposition data. In principle, we could attempt to introduce the full set of precipitation

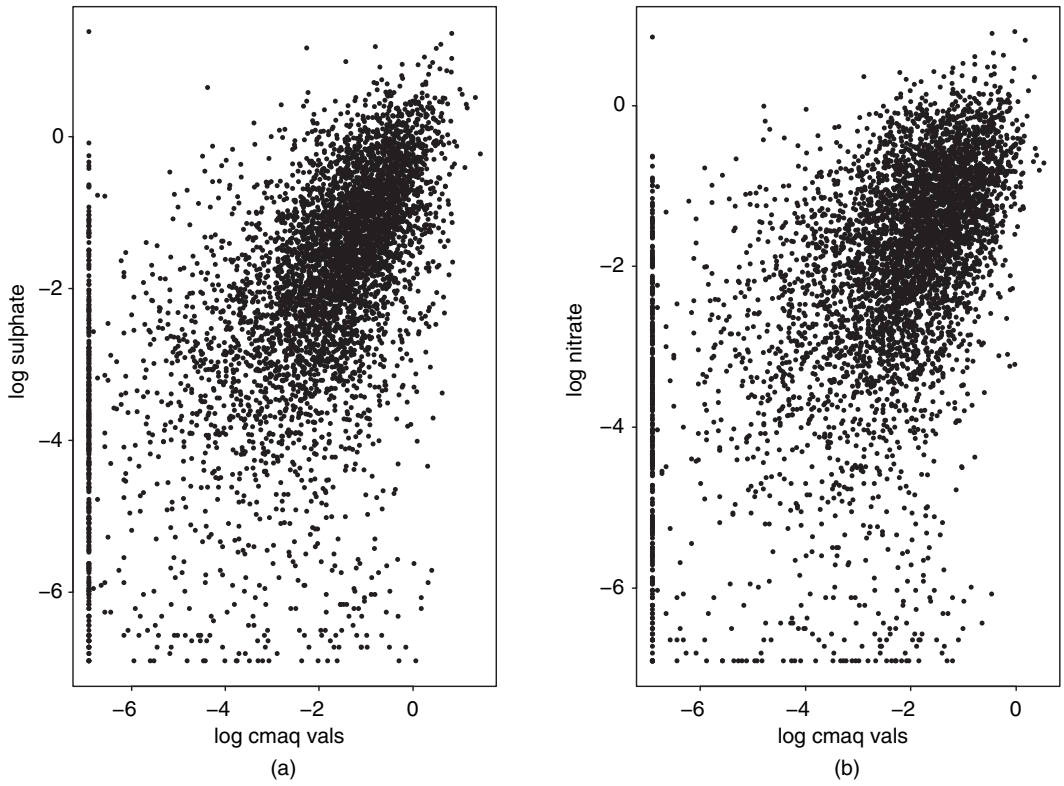

Fig. 5. Deposition at the NADP sites against the CMAQ values in the grid cell covering the corresponding NADP site on the log-scale: (a) wet sulphate; (b) wet nitrate

data into our modelling but this will add substantially to the computation (see expression (6) in Section 3.2) with little expected gain.

We have examined empirical variograms and their smoothed fits for many different versions of aggregated data as well as for residuals after fitting regression models for log-deposition values on log-precipitation and log-CMAQ values. The variograms revealed clear evidence of spatial dependence and suggested ranges between 500 and 1500 km. In our model fitting we choose optimal values of the range parameters by using validation methods. Throughout the paper we use the geodetic distance (see, for example, Banerjee *et al.* (2004), chapter 1) between two locations with given latitudes and longitudes.

3. Modelling wet deposition

We develop the wet deposition model in two stages described in Sections 3.1 and 3.2 respectively and provide a directed acyclic graph in Fig. 6. At the end of Section 3.2 we briefly discuss what a fusion model using block averaging (as in equation (1)) would look like, with an associated directed acyclic graph in Fig. 7. Section 3.3 discusses the prior distributions and records the joint posterior distribution.

3.1. First-stage specification

Let $P(\mathbf{s}_i, t)$ and $Z(\mathbf{s}_i, t)$ denote the observed precipitation and deposition (either sulphate or

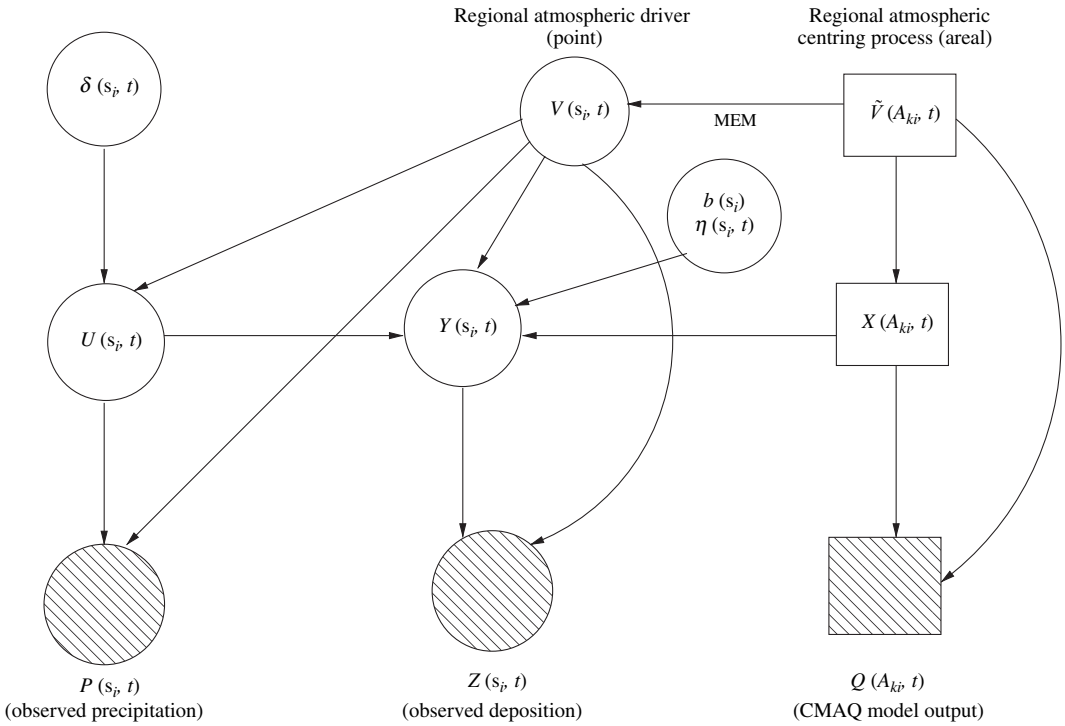

Fig. 6. Graphical representation of the model (the MEM handles $Q(A_{k_j}, t) > 0$, $Z(\mathbf{s}_j, t) = 0$ or $Q(A_{k_j}, t) = 0$, $Z(\mathbf{s}_j, t) > 0$): ○, ▨, point level random variable; □, ▧, areal level random variable; ▨, ▧, observed random variables; ○, □, latent unobserved variable

nitrate) respectively at a site $\mathbf{s}_i$, $i = 1, \ldots, n$, in week t, $t = 1, \ldots, T$. We suppose that $P(\mathbf{s}_i, t)$ and $Z(\mathbf{s}_i, t)$ are driven by a conceptual point level latent atmospheric process, denoted by $V(\mathbf{s}_i, t)$, and both take the value 0 if $V(\mathbf{s}_i, t) < 0$ to reflect that there is no deposition without precipitation, i.e.

$$P(\mathbf{s}_i, t) = \begin{cases} \exp\{U(\mathbf{s}_i, t)\} & \text{if } V(\mathbf{s}_i, t) > 0, \\ 0 & \text{otherwise,} \end{cases} \tag{2}$$

and

$$Z(\mathbf{s}_i, t) = \begin{cases} \exp\{Y(\mathbf{s}_i, t)\} & \text{if } V(\mathbf{s}_i, t) > 0, \\ 0 & \text{otherwise.} \end{cases} \tag{3}$$

The random variables $U(\mathbf{s}_i, t)$ and $Y(\mathbf{s}_i, t)$ are thus taken as log(observed precipitation) and log(observed deposition) respectively when $V(\mathbf{s}_i, t) > 0$. The models that are described below will specify their values when $V(\mathbf{s}_i, t) \leqslant 0$ and/or the corresponding $P(\mathbf{s}_i, t)$ or $Z(\mathbf{s}_i, t)$ are missing. Introduction of the $V(\mathbf{s}_i, t)$ process is made to accommodate the point masses; a model without the Vs, e.g. setting $P(\mathbf{s}_i, t) = \exp\{U(\mathbf{s}_i, t)\}$ if and only if $U(\mathbf{s}_i, t) > 0$, implies a discontinuity in $P(\mathbf{s}_i, t)$ at $U(\mathbf{s}_i, t) = 0$.

Let $Q(A_j, t)$ denote the CMAQ model output at grid cell A_j for week t, $j = 1, \ldots, J$. Similarly to expression (3) we suppose that $Q(A_j, t)$ is positive if a conceptual areal level latent atmospheric process, denoted by $\tilde{V}(A_j, t)$, is positive,

$$Q(A_j, t) = \begin{cases} \exp\{X(A_j, t)\} & \text{if } \tilde{V}(A_j, t) > 0, \\ 0 & \text{otherwise.} \end{cases} \tag{4}$$

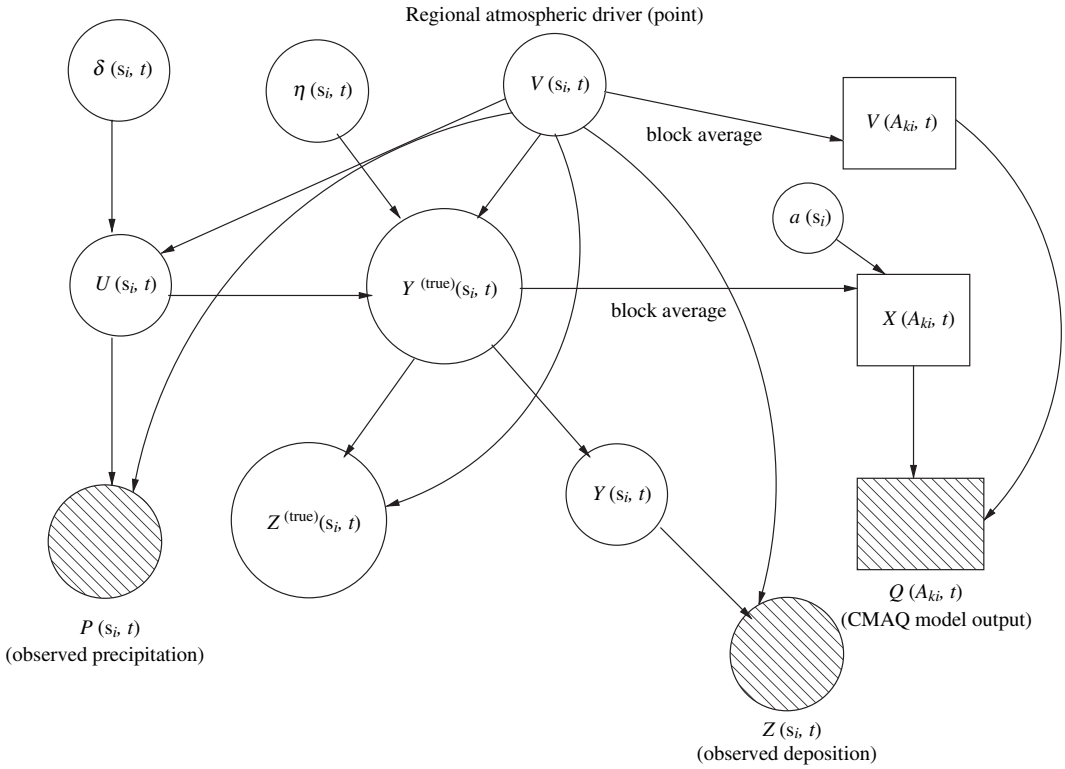

Fig. 7. Graphical representation of a fusion model: block averaging avoids the need for MEM; there is no $\tilde{V}(A_{k_i}, t)$ process

The values of $X(A_j, t)$ when $\tilde{V}(A_j, t) \leqslant 0$ will be given by the model that is described below. As computer model output, there are no missing values in the $Q(A_j, t)$.

Let **P**, **Z** and **Q** denote all the precipitation values, wet deposition values and the CMAQ model output respectively. Similarly define the vectors **U**, **Y** and **X** collecting all the elements of the corresponding random variable for $i = 1, \ldots, n$ and $t = 1, \ldots, T$. Let **V** and $\tilde{\mathbf{V}}$ denote the vectors collecting the elements $V(\mathbf{s}_i, t)$, $i = 1, \ldots, n$, and $\tilde{V}(A_j, t)$, $j = 1, \ldots, J$, respectively, for $t = 1, \ldots, T$.

The first-stage likelihood that is implied by the definitions (2)–(4) is given by

$$f(\mathbf{P}, \mathbf{Z}, \mathbf{Q} | \mathbf{U}, \mathbf{Y}, \mathbf{X}, \mathbf{V}, \tilde{\mathbf{V}}) = f(\mathbf{P} | \mathbf{U}, \mathbf{V})\, f(\mathbf{Z} | \mathbf{Y}, \mathbf{V})\, f(\mathbf{Q} | \mathbf{X}, \tilde{\mathbf{V}}) \tag{5}$$

which takes the form

$$\prod_{t=1}^{T} \left(\prod_{i=1}^{n} [\mathbf{1}_{\exp\{u(\mathbf{s}_i,t)\}} \mathbf{1}_{\exp\{y(\mathbf{s}_i,t)\}} I\{v(\mathbf{s}_i, t) > 0\}] \prod_{j=1}^{J} [\mathbf{1}_{\exp\{x(A_j,t)\}} I\{\tilde{v}(A_j, t) > 0\}] \right)$$

where $\mathbf{1}_x$ denotes a degenerate distribution with point mass at x and $I(\cdot)$ is the indicator function.

3.2. Second-stage specification

In the second stage of modelling we begin by specifying a spatially coloured regression model for log-precipitation based on the latent process $V(\mathbf{s}_i, t)$. In particular, we assume the model

$$U(\mathbf{s}_i, t) = \alpha_0 + \alpha_1 V(\mathbf{s}_i, t) + \delta(\mathbf{s}_i, t), \tag{6}$$

where $\boldsymbol{\delta}_t = (\delta(\mathbf{s}_1, t), \ldots, \delta(\mathbf{s}_n, t))'$ for $t = 1, \ldots, T$ is an independent Gaussian process following the $N(\mathbf{0}, \Sigma_\delta)$ distribution; Σ_δ has elements $\sigma_\delta(i, j) = \sigma_\delta^2 \exp(-\phi_\delta d_{ij})$, which is the usual exponential covariance function, where d_{ij} is the geodetic distance between sites $\mathbf{s}_i$ and $\mathbf{s}_j$. Using vector notation, this specification is equivalently written as

$$\mathbf{U}_t \sim N(\alpha_0 \mathbf{1} + \alpha_1 \mathbf{V}_t, \Sigma_\delta)$$

where $\mathbf{U}_t = (U(\mathbf{s}_1, t), \ldots, U(\mathbf{s}_n, t))'$ and $\mathbf{V}_t = (V(\mathbf{s}_1, t), \ldots, V(\mathbf{s}_n, t))'$ and $\mathbf{1}$ denotes a vector with all elements 1 (of appropriate order).

To model $Y(\mathbf{s}_i, t)$, we assume that

$$Y(\mathbf{s}_i, t) = \beta_0 + \beta_1 U(\mathbf{s}_i, t) + \beta_2 V(\mathbf{s}_i, t) + \{b_0 + b(\mathbf{s}_i)\} X(A_{k_i}, t) + \eta(\mathbf{s}_i, t) + \varepsilon(\mathbf{s}_i, t), \tag{7}$$

for $i = 1, \ldots, n$ and $t = 1, \ldots, T$ where, unless otherwise mentioned, A_{k_i} is the grid cell which contains the site $\mathbf{s}_i$.

The error terms $\varepsilon(\mathbf{s}_i, t)$ are assumed to follow $N(0, \sigma_\varepsilon^2)$ independently, providing the so-called nugget effect. The reasoning for the rest of the specification in equation (7) is as follows. The term $\beta_1 U(\mathbf{s}_i, t)$ is included because of the strong linear relationships between log-deposition and log-precipitation; see Fig. 4. The term $\beta_2 V(\mathbf{s}_i, t)$ captures any direct influence of the atmospheric process $V(\mathbf{s}_i, t)$ on $Y(\mathbf{s}_i, t)$ in the presence of precipitation.

The exploratory analyses that were presented earlier also provided evidence for possible linear relationships between log-deposition and log-CMAQ values. To specify a rich class of *locally* linear models we may think of a spatially varying slope for the regression of $Y(\mathbf{s}_i, t)$ on log-CMAQ values $X(A_j, t)$, which is specified as $\{b_0 + b(\mathbf{s}_i)\} X(A_{k_i}, t)$ in equation (7). Writing $\mathbf{b} = (b(\mathbf{s}_1), \ldots, b(\mathbf{s}_n))'$ we propose a mean 0 Gaussian process for $\mathbf{b}$, i.e.

$$\mathbf{b} \sim N(\mathbf{0}, \Sigma_b)$$

where Σ_b has elements $\sigma_b(i, j) = \sigma_b^2 \exp(-\phi_b d_{ij})$.

The term $\eta(\mathbf{s}_i, t)$ provides a spatially varying intercept which can also be interpreted as a spatiotemporal adjustment to the overall intercept parameter β_0. We assume that

$$\boldsymbol{\eta}_t \sim N(\mathbf{0}, \Sigma_\eta), \qquad t = 1, \ldots, T,$$

independently where $\boldsymbol{\eta}_t = (\eta(\mathbf{s}_1, t), \ldots, \eta(\mathbf{s}_n, t))'$ and Σ_η has elements $\sigma_\eta(i, j) = \sigma_\eta^2 \exp(-\phi_\eta d_{ij})$. We can consider replacing $\eta(\mathbf{s}_i, t)$ with $\eta(\mathbf{s}_i)$. The pure spatial term will fail to capture the between-week variability in the intercept; see Carroll *et al.* (1997) for a related discussion. However, it does provide a common term for all weekly predictions yielding possibly appropriate increased uncertainty in long-term averaging; see Stein's discussion to Carroll *et al.* (1997).

The regression model (7) is now equivalently written as

$$\mathbf{Y}_t \sim N(\boldsymbol{\vartheta}_t, \sigma_\varepsilon^2 I_n)$$

where $\mathbf{Y}_t = (Y(\mathbf{s}_1, t), \ldots, Y(\mathbf{s}_n, t))'$ and $\boldsymbol{\vartheta}_t = \beta_0 \mathbf{1} + \beta_1 \mathbf{U}_t + \beta_2 \mathbf{V}_t + b_0 \mathbf{X}_t + X_t \mathbf{b} + \boldsymbol{\eta}_t$ where $\mathbf{X}_t$ is the n-dimensional vector with ith element given by $X(A_{k_i}, t)$ and X_t is a diagonal matrix whose ith diagonal entry is $X(A_{k_i}, t)$, $i = 1, \ldots, n$, and I_n is the identity matrix of order n.

The CMAQ output $X(A_j, t)$ is modelled by using the latent process $\tilde{V}(A_j, t)$ as follows:

$$X(A_j, t) = \gamma_0 + \gamma_1 \tilde{V}(A_j, t) + \psi(A_j, t), \qquad j = 1, \ldots, J, \tag{8}$$

where $\psi(A_j, t) \sim N(0, \sigma_\psi^2)$ independently for all $j = 1, \ldots, J$, $t = 1, \ldots, T$ and σ_ψ^2 is unknown. In vector notation, this is given by

$$\mathbf{X}_t \sim N(\gamma_0 \mathbf{1} + \gamma_1 \tilde{\mathbf{V}}_t, \sigma_\psi^2 I_J)$$

where $\mathbf{X}_t = (X(A_1,t),\ldots X(A_J,t))'$ and $\tilde{\mathbf{V}}_t = (\tilde{V}(A_1,t),\ldots \tilde{V}(A_J,t))'$; see the partitioning of $\tilde{\mathbf{V}}_t$ below equation (9) regarding the order of the grid cell indices $1,\ldots,J$.

We now turn to specification of the latent processes $V(\mathbf{s}_i,t)$ and $\tilde{V}(A_j,t)$. Note that it is possible to have $Z(\mathbf{s}_i,t)>0$ and $Q(A_{k_i},t)=0$ and vice versa since $Q(A_{k_i},t)$ is the output of a computer model which has not used the actual observation $Z(\mathbf{s}_i,t)$. This implies that $V(\mathbf{s}_i,t)$ and $\tilde{V}(A_{k_i},t)$ can be of different signs. To accommodate this flexibility and to distinguish between the point and areal processes we assume the simple measurement error model:

$$V(\mathbf{s}_i,t) \sim N\{\tilde{V}(A_{k_i},t), \sigma_v^2\}, \tag{9}$$

for $i=1,\ldots,n$ and $t=1,\ldots,T$, where σ_v^2 is unknown. Without loss of generality we write $\tilde{\mathbf{V}}_t = (\tilde{\mathbf{V}}_t^{(1)}, \tilde{\mathbf{V}}_t^{(2)})'$ where the n-dimensional vector $\tilde{\mathbf{V}}_t^{(1)}$ contains the values for the grid cells where the n observation sites are located and $\tilde{\mathbf{V}}_t^{(2)}$ contains the values for the remaining $J-n$ grid cells. The specification (9) can now be written equivalently as

$$\mathbf{V}_t \sim N(\tilde{\mathbf{V}}_t^{(1)}, \sigma_v^2 I_n), \qquad t=1,\ldots,T.$$

The latent process $\tilde{V}(A_j,t)$ is assumed to follow a first-order auto-regressive process in time and a CAR process in space, i.e.

$$\tilde{V}(A_j,t) = \rho\, \tilde{V}(A_j,t-1) + \zeta(A_j,t) \tag{10}$$

for $j=1,\ldots,J$ and $t=1,\ldots,T$. The $\zeta(A_j,t)$ are independent improper CAR models (see for example Banerjee *et al.* (2004)) over t, i.e.

$$\zeta(A_j,t) \sim N\left\{ \sum_{i=1}^{J} h_{ji}\,\zeta(A_i,t), \frac{\sigma_\zeta^2}{m_j} \right\} \tag{11}$$

where

$$h_{ji} = \begin{cases} 1/m_j & \text{if } i \in \partial_j, \\ 0 & \text{otherwise} \end{cases}$$

and ∂_j defines the m_j neighbouring grid cells of the cell A_j.

We initiate the process (10) with

$$\tilde{V}(A_j,0) = \frac{1}{T}\sum_{t=1}^{T} X(A_j,t),$$

the mean of the observed $X(A_j,t)$ values. Now we have the temporally vectorized auto-regressive and spatially CAR specification:

$$f(\tilde{\mathbf{V}}_t|\tilde{\mathbf{V}}_{t-1},\rho,\sigma_\zeta^2) \propto \exp\{-\tfrac{1}{2}(\tilde{\mathbf{V}}_t - \rho\tilde{\mathbf{V}}_{t-1})' D^{-1}(I-H)(\tilde{\mathbf{V}}_t - \rho\tilde{\mathbf{V}}_{t-1})\} \tag{12}$$

where D is diagonal with the jth diagonal entry given by σ_ζ^2/m_j. In summary, the second-stage specification is given by

$$\prod_{t=1}^{T} \{ f(\mathbf{Y}_t|\mathbf{U}_t,\mathbf{V}_t,\mathbf{X}_t,\boldsymbol{\eta}_t,\mathbf{b},\boldsymbol{\theta})\, f(\boldsymbol{\eta}_t|\boldsymbol{\theta})\, f(\mathbf{U}_t|\mathbf{V}_t,\boldsymbol{\theta})\, f(\mathbf{V}_t|\tilde{\mathbf{V}}_t^{(1)},\boldsymbol{\theta}) \times f(\mathbf{X}_t|\tilde{\mathbf{V}}_t,\boldsymbol{\theta})\, f(\tilde{\mathbf{V}}_t|\tilde{\mathbf{V}}_{t-1},\boldsymbol{\theta})\}\, f(\mathbf{b}|\boldsymbol{\theta})$$

where $\boldsymbol{\theta}$ denote the parameters α_0, α_1, β_0, β_1, β_2, b_0, γ_0, γ_1, ρ, σ_δ^2, σ_b^2, σ_η^2, σ_ε^2, σ_ψ^2, σ_v^2 and σ_ζ^2. Fig. 6 provides a directed graphical model for our entire specification, noting the measurement error specification.

As noted in Section 1, hierarchical modelling for fusion between monitoring data and model output data has been proposed in Fuentes and Raftery (2005). Their approach introduces a

model for latent true deposition $Z^{(\text{true})}(\mathbf{s}_i, t)$. In our setting the true deposition would be driven by a regional atmospheric process as in Section 3.1. To connect the process to the grid cell model output data, block averaging is required. Fig. 7 shows the analogue of our modelling using this approach. The key point is the direction arrow linking the $V(\mathbf{s}_i, t)$ and the $\tilde{V}(A_{k_i}, t)$, an MEM *versus* block averaging. Hence, the infeasibility of fitting the model in Fig. 7 in the case of a large number of grid cells emerges. For the CMAQ output that we use, 33 390 block averages are required, and, in fact, these are required for each $t = 1, \ldots, 52$ weeks. (We note further that the fusion model of Fuentes and Raftery (2005) has not actually been implemented in a dynamic setting.) The advantage of the model in Fig. 6 is clear. We must only fit the measurement error model to the 120 monitoring sites while doing cheap CAR updates for the $\tilde{V}$s. Generally, our approach will be preferred for environmental data settings since there will always be many more grid cells than monitoring stations, and this will be further exacerbated by computer models seeking higher spatial resolution.

We attempt further clarification of the V- and $\tilde{V}$-processes as well as justification for the measurement model (9). Again, our specification does not view $\tilde{V}(A_{k_i}, t)$ as a block average of $V(\mathbf{s}_i, t)$ over A_{k_i}. Rather, it views $V(\mathbf{s}_i, t) - \tilde{V}(A_{k_i}, t)$ as a deviation from the areal average and we assume that these are independent across the $\mathbf{s}_i$ where V and $\tilde{V}$ are two distinct mean 0 spatial processes operating at different spatial scales. Careful algebraic calculation, using the models in expressions (6)–(10), shows that $(U(\mathbf{s}_i, t), Y(\mathbf{s}_i, t))$ given $V(\mathbf{s}_i, t)$ and $X(A_{k_i}, t)$ is a bivariate space–time Gaussian process which is captured through point level space–time random effects, $\delta(\mathbf{s}_i, t)$ and $\eta(\mathbf{s}_i, t)$. But, under the models for $V(\mathbf{s}_i, t)|\tilde{V}(A_{k_i}, t)$ and $X(A_{k_i}, t)|\tilde{V}(A_{k_i}, t)$, we can marginalize over V and X to obtain a marginal bivariate Gaussian process, $(U(\mathbf{s}_i, t), Y(\mathbf{s}_i, t))$ given $\tilde{V}$. In other words, the $\tilde{V}(A_{k_i}, t)$ introduces spatial random effects at the areal unit scale. So, the overall specification is a multiscale space–time process with uncorrelated effects introduced in an additive manner. Such specifications have a long history in geostatistics (see, for example, Goulard and Voltz (1992) and Gotway and Young (2002)). Adopting such a specification is a familiar device for avoiding block averaging.

3.3. Prior and posterior distributions

We now complete the Bayesian model specification by assuming prior distributions for all the unknown parameters. We assume that, *a priori*, each of α_0, α_1, β_0, β_1, β_2, b_0, γ_0, γ_1, and ρ is normally distributed with mean 0 and variance 10^4, which is essentially a flat prior specification. The inverse of the variance components $1/\sigma_\delta^2$, $1/\sigma_b^2$, $1/\sigma_\eta^2$, $1/\sigma_\varepsilon^2$, $1/\sigma_\psi^2$, $1/\sigma_v^2$ and $1/\sigma_\zeta^2$ are all assumed to follow the gamma distribution $G(\nu, \lambda)$ having mean ν/λ. In our implementation we take $\nu = 2$ and $\lambda = 1$, implying that these variance components have prior mean 1 and infinite variance.

The logarithm of the likelihood times the prior in the second stage conditional on the decay parameter values and up to an additive constant is given by

$$
\begin{aligned}
&-\frac{nT}{2}\log(\sigma_\varepsilon^2) - \frac{1}{2\sigma_\varepsilon^2}\sum_{t=1}^{T}(\mathbf{y}_t - \boldsymbol{\vartheta}_t)'(\mathbf{y}_t - \boldsymbol{\vartheta}_t) - \frac{nT}{2}\log(\sigma_\eta^2) - \frac{1}{2\sigma_\eta^2}\sum_{t=1}^{T}\boldsymbol{\eta}_t' S_\eta^{-1}\boldsymbol{\eta}_t \\
&\quad -\frac{nT}{2}\log(\sigma_\delta^2) - \frac{1}{2\sigma_\delta^2}\sum_{t=1}^{T}(\mathbf{u}_t - \alpha_0\mathbf{1} - \alpha_1\mathbf{v}_t)' S_\delta^{-1}(\mathbf{u}_t - \alpha_0\mathbf{1} - \alpha_1\mathbf{v}_t) \\
&\quad\quad -\frac{nT}{2}\log(\sigma_v^2) - \frac{1}{2\sigma_v^2}\sum_{t=1}^{T}(\mathbf{v}_t - \tilde{\mathbf{v}}_t^{(1)})'(\mathbf{v}_t - \tilde{\mathbf{v}}_t^{(1)})' \\
&\quad -\frac{JT}{2}\log(\sigma_\psi^2) - \frac{1}{2\sigma_\psi^2}\sum_{t=1}^{T}(\mathbf{x}_t - \gamma_0\mathbf{1} - \gamma_1\tilde{\mathbf{v}}_t)'(\mathbf{x}_t - \gamma_0\mathbf{1} - \gamma_1\tilde{\mathbf{v}}_t)
\end{aligned}
$$

$$-\frac{JT}{2}\log(\sigma_\zeta^2)-\frac{1}{2}\sum_{t=1}^{T}(\tilde{\mathbf{v}}_t-\rho\tilde{\mathbf{v}}_{t-1})'D^{-1}(I-H)\left(\tilde{\mathbf{v}}_t-\rho\tilde{\mathbf{v}}_{t-1}\right)$$
$$-\frac{n}{2}\log(\sigma_b^2)-\frac{1}{2\sigma_b^2}\mathbf{b}'S_b^{-1}\mathbf{b}+\log\{f(\boldsymbol{\theta})\}$$

where $f(\boldsymbol{\theta})$ is the prior distribution of $\boldsymbol{\theta}$ and $\Sigma_\delta=\sigma_\delta^2 S_\delta, \Sigma_b=\sigma_b^2 S_b$ and $\Sigma_\eta=\sigma_\eta^2 S_\eta$. The choice of the decay parameters is discussed below.

3.4. Choice of the decay parameters

Ideally, $\boldsymbol{\phi}=(\phi_\delta,\phi_b,\phi_\eta)$ should be estimated within the Bayesian model as well. However, in a classical inference setting it is not possible to estimate both ϕ and σ^2 consistently in a typical model for spatial data with a covariance function belonging to the Matérn family; see Zhang (2004). Moreover, Stein (1999) showed that spatial interpolation is sensitive to the product $\sigma^2\phi$ but not to either parameter individually. In our Bayesian inference set-up using Gibbs sampling, joint estimation is often poorly behaved because of weak identifiability and extremely slow mixing of the associated Markov chains under vague prior distributions for $\boldsymbol{\phi}$. In addition, the full conditional distribution for each of the decay parameters is not conjugate so sampling them in a Gibbs sampler requires expensive likelihood evaluations in each iteration. These difficulties are exacerbated by the large volume of data that we model here. See, for example, Sahu *et al.* (2006, 2007) and references therein for more in this regard.

Thus, with little interest in the $\boldsymbol{\phi}$ and with little ability for the data to inform about them, and in the interest of well-behaved model fitting, we use an empirical Bayes approach based on the set-aside validation data from eight stations to select $\boldsymbol{\phi}$. We search for optimal values of $\boldsymbol{\phi}$ in a three-dimensional grid by using the validation mean-square error VMSE given by

$$\text{VMSE}=\frac{1}{n_v}\sum_{i=1}^{8}\sum_{t=1}^{T}\{Z(\mathbf{s}_i^*,t)-\hat{Z}(\mathbf{s}_i^*,t)\}^2\, I\{Z(\mathbf{s}_i^*,t)\} \tag{13}$$

where $\hat{Z}(\mathbf{s}_i^*,t)$ denotes the model-based validation prediction estimate (see Section 4 for details) for $Z(\mathbf{s}_i^*,t)$; $\mathbf{s}_i^*$ denotes the ith validation site; $I\{Z(\mathbf{s}_i^*,t)\}$ equals 1 if $Z(\mathbf{s}_i^*,t)$ has been observed and 0 otherwise, and n_v is the total number of available observations at the eight validation sites. For our data set $n_v=407$ since there were nine missing observations; see Section 2.

We searched for the optimal values of ϕ_η, ϕ_δ and ϕ_b in a three-dimensional grid formed of the values 0.002, 0.003, 0.006, 0.012 and 0.06 corresponding to spatial ranges of 1500, 1000, 500, 250 and 50 km, separately for the sulphate and nitrate deposition models. (The data cannot be expected to inform about the range to a finer resolution.) The combination of values $\phi_\eta=0.006$, $\phi_\delta=0.003$ and $\phi_b=0.006$ provided the best VMSE-values for both the sulphate and the nitrate model. The corresponding optimal ranges are 500, 1000 and 500 km respectively. VMSE is not at all sensitive to the choice of the decay parameters near these best values. As a result, although it is possible to refine the grid in a neighbourhood of the best value further we do not explore beyond our grid here. In fact, this insensitivity is also supported by our investigation of the empirical variograms that were discussed in Section 2. Estimation of the remaining parameters proceeds conditionally on the optimal choice of $\boldsymbol{\phi}$.

4. Predicting deposition at a new location

The models that were developed in Section 3 allow us to interpolate the spatial deposition surface at any given week in the year. Consider the problem of predicting $Z(\mathbf{s}',t')$ in week t' at any new

location $\mathbf{s}'$ falling on the grid cell A'. The prediction is performed by constructing the posterior predictive distribution of $Z(\mathbf{s}', t')$ which in turn depends on the distribution of $Y(\mathbf{s}', t')$ as specified by equation (7) along with the associated $V(\mathbf{s}', t')$. We estimate the posterior predictive distribution by drawing samples from it.

Several cases arise depending on the nature of information that is available at the new site $\mathbf{s}'$ at week t'. If precipitation information is available and there is no positive precipitation, i.e. $p(\mathbf{s}', t') = 0$, then we have $Z(\mathbf{s}', t') = 0$ and no further sampling is needed, since there can be no deposition without precipitation. Now suppose that there is positive precipitation, i.e. $p(\mathbf{s}', t') > 0$; then set $u(\mathbf{s}', t') = \log\{p(\mathbf{s}', t')\}$. We need to generate a sample $Y(\mathbf{s}', t')$. We first generate $V(\mathbf{s}', t') \sim N\{\tilde{V}(A', t'), \sigma_v^2\}$ following the measurement error model (9). Note that $\tilde{V}(A', t')$ is already available for any grid cell A' (within the study region) and week t' (in the current year) from model fitting; see equation (10). Similarly, $X(A', t')$ is also available either as the logarithm of the CMAQ output, $\log\{Q(A', t')\}$, if $Q(A', t') > 0$ or from the Markov chain Monte Carlo (MCMC) imputation when $Q(A', t') = 0$; see Appendix A. To sample $\eta(\mathbf{s}', t')$ we note that

$$\begin{pmatrix} \eta(\mathbf{s}', t') \\ \boldsymbol{\eta}_{t'} \end{pmatrix} \sim N\left\{ \begin{pmatrix} 0 \\ \mathbf{0} \end{pmatrix}, \sigma_\eta^2 \begin{pmatrix} 1 & S_{\eta,12} \\ S_{\eta,21} & S_\eta \end{pmatrix} \right\},$$

where $S_{\eta,12}$ is $1 \times n$ with the ith entry given by $\exp\{-\phi_\eta\, d(\mathbf{s}_i, \mathbf{s}')\}$ and $S_{\eta,21} = S'_{\eta,12}$. Therefore,

$$\eta(\mathbf{s}', t') | \boldsymbol{\eta}_{t'}, \boldsymbol{\theta} \sim N\{S_{\eta,12} S_\eta^{-1} \boldsymbol{\eta}_{t'}, \sigma_\eta^2 (1 - S_{\eta,12} S_\eta^{-1} S_{\eta,21})\}. \tag{14}$$

If the term $b(\mathbf{s})$ is included in the model we need to simulate $b(\mathbf{s}')$ conditional on $\mathbf{b}$ and model parameters. To do this we note that

$$\begin{pmatrix} b(\mathbf{s}') \\ \mathbf{b} \end{pmatrix} \sim N\left\{ \begin{pmatrix} 0 \\ \mathbf{0} \end{pmatrix}, \sigma_b^2 \begin{pmatrix} 1 & S_{b,12} \\ S_{b,21} & S_b \end{pmatrix} \right\},$$

where $S_{b,12}$ is $1 \times n$ with the ith entry given by $\exp\{-\phi_\eta\, d(\mathbf{s}_i, \mathbf{s}')\}$ and $S_{b,21} = S'_{b,12}$. Therefore,

$$b(\mathbf{s}') | \boldsymbol{\theta} \sim N\{S_{b,12} S_b^{-1} \mathbf{b}, \sigma_b^2 (1 - S_{b,12} S_b^{-1} S_{b,21})\}. \tag{15}$$

If it is desired to predict $Z(\mathbf{s}', t')$ where $P(\mathbf{s}', t')$ is not available, we proceed as follows. We generate $V(\mathbf{s}', t') \sim N\{\tilde{V}(A', t'), \sigma_v^2\}$ following the measurement error model (9). If this $V(\mathbf{s}', t') < 0$, then we set both $p(\mathbf{s}', t')$ and $Z(\mathbf{s}', t')$ to 0. If, however, $V(\mathbf{s}', t') > 0$ we need additionally to draw $U(\mathbf{s}', t')$ by using the precipitation model (6). For this we note that

$$\begin{pmatrix} U(\mathbf{s}', t') \\ \mathbf{U}_{t'} \end{pmatrix} \sim N\left\{ \begin{pmatrix} \alpha_0 + \alpha_1 V(\mathbf{s}', t') \\ \alpha_0 \mathbf{1} + \alpha_1 \mathbf{V}_{t'} \end{pmatrix}, \sigma_\delta^2 \begin{pmatrix} 1 & S_{\delta,12} \\ S_{\delta,21} & S_\delta \end{pmatrix} \right\},$$

where $S_{\delta,12}$ is $1 \times n$ with the ith entry given by $\exp\{-\phi_\delta\, d(\mathbf{s}_i, \mathbf{s}')\}$ and $S_{\delta,21} = S'_{\delta,12}$. Therefore,

$$U(\mathbf{s}', t') | \mathbf{U}_{t'}, \boldsymbol{\theta} \sim N\{\mu(\mathbf{s}', t'), \sigma_\delta^2 (1 - S_{\delta,12} S_\delta^{-1} S_{\delta,21})\}, \tag{16}$$

where

$$\mu(\mathbf{s}', t') = \alpha_0 + \alpha_1\, V(\mathbf{s}', t') + S_{\delta,12} S_\delta^{-1} (\mathbf{U}_{t'} - \alpha_0 \mathbf{1} - \alpha_1 \mathbf{v}_{t'}).$$

If $Z(\mathbf{s}', t')$ is not inferred to be 0 then we set it to be $\exp\{Y(\mathbf{s}', t')\}$. If we want the predictions of the smooth deposition surface without the nugget term we simply ignore the nugget term $\varepsilon(\mathbf{s}', t')$ in generating $Y(\mathbf{s}', t')$. Annual and quarterly predictions at a location $\mathbf{s}'$ are obtained by forming sums of $Z(\mathbf{s}', t')$ appropriately; for example the annual deposition is $g(\mathbf{s}') = \Sigma_{t'=1}^{T} Z(\mathbf{s}', t')$. Thus at each MCMC iteration j we have $Z^{(j)}(\mathbf{s}', t')$ and $g^{(j)}(\mathbf{s}')$. We use the median of the accumulated MCMC samples and the lengths of the 95% intervals to summarize the predictions. The median as a summary measure preserves the one-to-one relationships between summaries for Y and

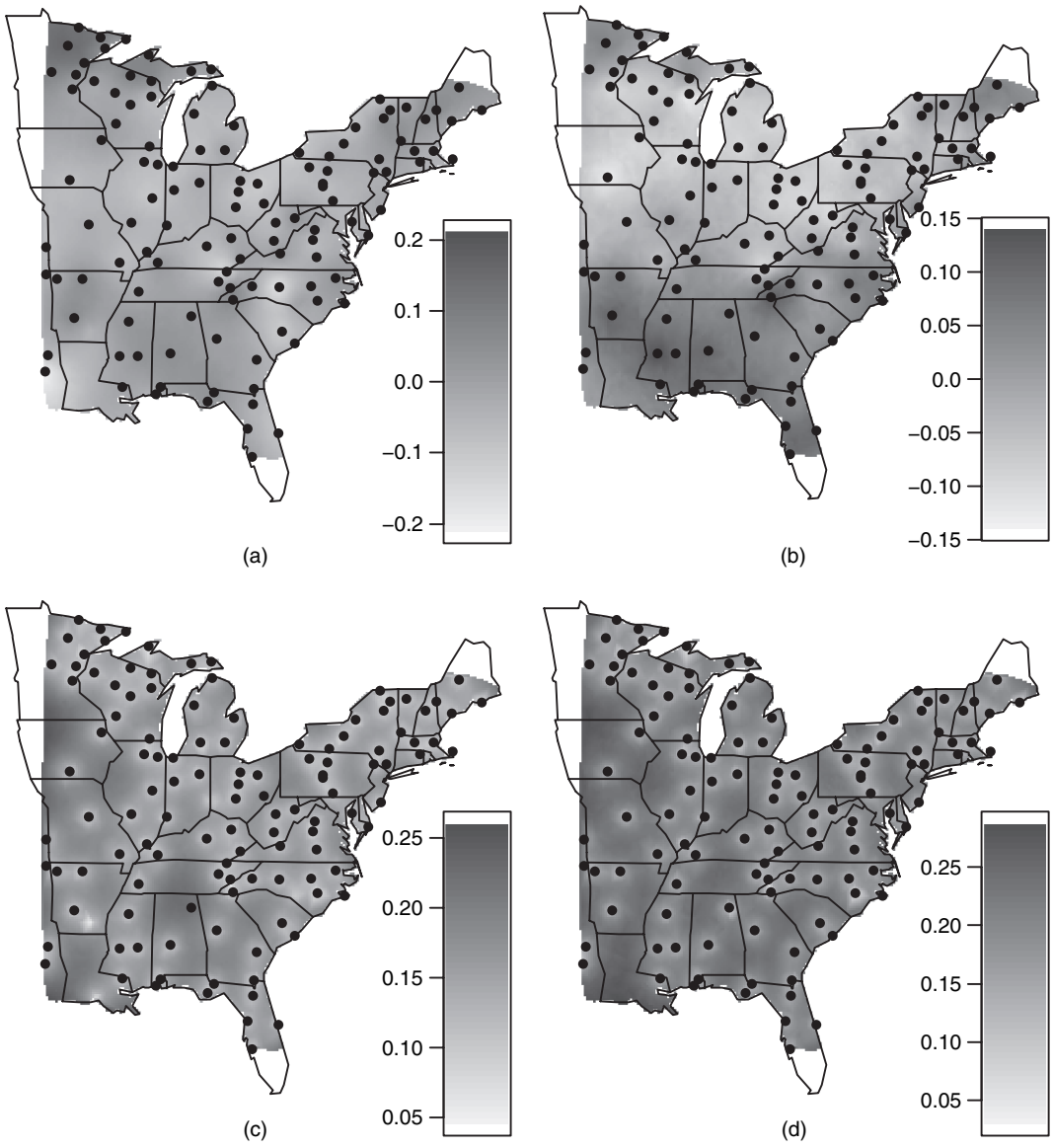

Fig. 8. $b(\mathbf{s})$ surface for sulphate, (b) $b(\mathbf{s})$ surface for nitrate, (c) standard deviations of the $b(\mathbf{s})$ surface for sulphate and (d) standard deviations of the $b(\mathbf{s})$ surface for nitrate

Z. Exploratory data analyses of the MCMC output showed rapid convergence for the models adopted. For making inference, we used 10000 MCMC iterations after discarding the first 5000 iterations.

5. Analysis

5.1. Model choice and validation

For model choice we compared several possible models by using the predictive Bayesian model selection criterion of Gelfand and Ghosh (1998). The additional term $b(\mathbf{s}_i)\, X(A_{k_i}, t)$ did not

improve model fitting greatly. Only a few $b(\mathbf{s}_i)$ were significant; see Fig. 8 where the estimated $b(\mathbf{s})$ surfaces along with their standard deviation surfaces have been plotted. Fig. 8 shows that the $b(\mathbf{s})$ values are very small in absolute value relative to the standard deviations. Moreover, the Gelfand and Ghosh criterion was much smaller for the model without the $b(\mathbf{s}_i)X(A_{k_i}, t)$ term. Henceforth, we worked with the submodel corresponding to $b(\mathbf{s}) = 0$. This is also explained by the fact that, after accounting for the very large influence of precipitation and a spatiotemporally varying intercept term, the model cannot detect a significant spatially varying contribution of the CMAQ output towards explaining deposition. This, however, *does not* mean that there is no spatiotemporal bias in the CMAQ output—such biases can simply be recovered by the differences between the model-based predictions and the CMAQ output. If the intention is to recover the bias by using a parametric form then a model omitting the most significant regressor, i.e. precipitation, must be specified.

For the purposes of model checking Fig. 9 provides predictions at the validation sites *versus* the observed values along with the validation prediction intervals on the original scale for all the 407 available observations in the eight validation sites. Note that more than one observation can assume the same value owing to truncation. Some negative bias is seen in sulphate prediction for very few (two or three out of 407) extreme large values which are very far out in the tail. This is not a major concern, however, since the corresponding predictive intervals are larger than the remaining intervals showing more uncertainty. Note also that these predictive intervals include the 45° line which shows that the bias is not statistically significant.

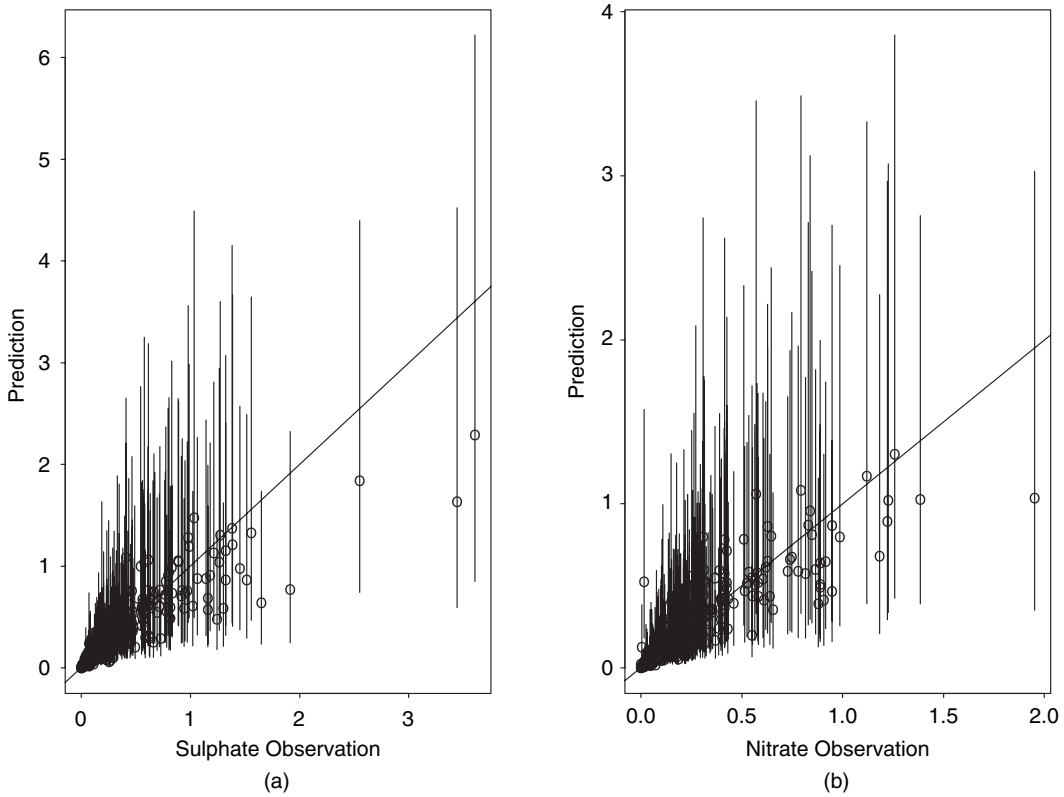

Fig. 9. Validations *versus* the observed values at the eight reserved sites (|, validation prediction interval): (a) wet sulphate; (b) wet nitrate

The overall VMSE is 0.035 for sulphate and 0.015 for nitrate, and 95% and 96% of the nominal 95% validation prediction intervals contain the true sulphate and nitrate depositions respectively. Overall, the validation analysis indicates that the model does not appear to introduce any bias in prediction and performs very well for out-of-sample predictions.

5.2. Results and interpretation

Table 1 provides the parameter estimates. There is a very strong effect of precipitation since the parameter β_1 is significant for both sulphate and nitrate. Note that β_2 is not significant (for both models), which is probably attributable to the fact that the regional atmospheric driver process influences deposition directly through precipitation. Although small, the significant estimates of b_0 indicate that the point level data and the gridded CMAQ output are strongly correlated, corroborating the exploratory analysis in Fig. 5. As expected the parameters α_1 and γ_1 are significant, showing that the point level atmospheric process is strongly related to precipitation and the areal level atmospheric process is a very good predictor of CMAQ output. There is strong temporal dependence between the CMAQ output in successive weeks (estimates of $\rho = 0.7688$ and $\rho = 0.7492$ for sulphate and nitrate respectively with standard deviation 0.0012 and 0.0013). The estimates of the variance components show that the magnitude of the nugget effect σ_ε^2 is the smallest. Hence more variation is explained by the spatiotemporal intercept process $\eta(\mathbf{s}, t)$ than the pure error process $\varepsilon(\mathbf{s}, t)$.

Maps of annual depositions are provided in Figs 10(a) and 11(a). For sulphate deposition the VMSE for the annual totals from the eight reserved sites for the IDW method is 20.4 whereas the same for our model is 8.1. The corresponding statistics for the nitrate deposition are 3.5 and 1.3. These show better performance by our model both for the sulphate and for the nitrate depositions. The highest wet sulphate deposition occurs near major emissions sources such as fossil-fuelled power plants (which are concentrated in the Ohio River Valley) and mobile

Table 1. Estimation of the parameters for the sulphate and nitrate models†

Parameter	*Results for sulphate deposition*			*Results for nitrate deposition*		
	Mean	*Standard deviation*	*95% CI*	*Mean*	*Standard deviation*	*95% CI*
α_0	−0.4497	0.0871	(−0.6189, −0.2733)	−0.3548	0.0596	(−0.4695, −0.2369)
α_1	0.1787	0.0379	(0.1017, 0.2499)	0.1522	0.0336	(0.0843, 0.2161)
β_0	−1.9414	0.0196	(−1.9784, −1.9012)	−1.9976	0.0192	(−2.0344, −1.9605)
β_1	0.9103	0.0067	(0.8972, 0.9240)	0.8412	0.0070	(0.8274, 0.8553)
β_2	0.0029	0.0062	(−0.0091, 0.0151)	0.0040	0.0060	(−0.0078, 0.0159)
b_0	0.0490	0.0053	(0.0386, 0.0599)	0.0535	0.0062	(0.0409, 0.0652)
γ_0	−3.0768	0.0035	(−3.0836, −3.0700)	−3.2177	0.0033	(−3.2242, −3.2112)
γ_1	0.8957	0.0034	(0.8891, 0.9025)	0.7368	0.0033	(0.7303, 0.7433)
ρ	0.7688	0.0012	(0.7664, 0.7712)	0.7492	0.0013	(0.7468, 0.7517)
σ_δ^2	2.6438	0.0602	(2.5254, 2.7631)	1.8694	0.0387	(1.7942, 1.9476)
σ_η^2	0.2812	0.0101	(0.2616, 0.3010)	0.3354	0.0105	(0.3149, 0.3564)
σ_ξ^2	0.0718	0.0057	(0.0607, 0.0832)	0.0727	0.0074	(0.0588, 0.0878)
σ_ψ^2	2.5062	0.0033	(2.4997, 2.5127)	2.2148	0.0028	(2.2092, 2.2203)
σ_υ^2	0.8087	0.0259	(0.7601, 0.8620)	0.7821	0.0237	(0.7366, 0.8290)
σ_ζ^2	0.4345	0.0011	(0.4322, 0.4367)	0.4340	0.0012	(0.4316, 0.4363)

†CI stands for equal-tailed credible intervals.

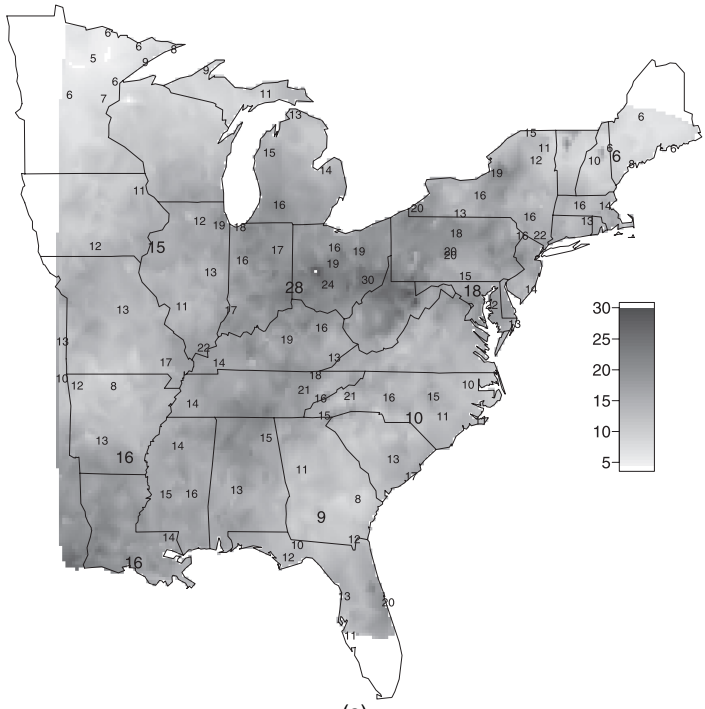

(a)

(b)

Fig. 10. Analyses for sulphate: (a) annual model-predicted map (the observed annual totals are labelled; a larger size of fount is used for the validation sites); (b) lengths of the prediction intervals

Fig. 11. Analyses for nitrate: (a) annual model-predicted map (the observed annual totals are labelled; a larger size of fount is used for the validation sites); (b) lengths of the prediction intervals

Fig. 12. Sulphate prediction maps on four quarters: (a) January–March; (b) April–June; (c) July–September; (d) October–December

sources in major population centres. Lower values occur near background monitoring sites. These 2001 patterns are similar to those reported by Brook *et al.* (1995) for eastern North America.

The lengths of the prediction intervals are provided as maps in Figs 10(d) and 11(d). As expected, the lengths are smaller for the predictive sites near the modelling sites and also for sites in the regions of low depositions.

The quarterly prediction maps are provided in Figs 12 and 13. Increased depositions are seen during the spring and summer months April–September analogously to the summary Fig. 3.

Fig. 13. Nitrate prediction maps on four quarters: (a) January–March; (b) April–June; (c) July–September; (d) October–December

The lengths of the predictions intervals, which are plotted in Figs 14 and 15, show that the uncertainties in quarterly maps are reasonably consistent over the seasons.

6. Discussion

The paper has developed a data fusion approach using a measurement error specification to combine gridded CMAQ output and point level monitoring data. Model components have been linked by using latent processes in a Bayesian hierarchical framework. We use this approach to investigate space–time wet deposition patterns over eastern USA. Compared with the current

Fig. 14. Maps showing the lengths of the 95% credible intervals for the sulphate predictions on four quarters: (a) January–March; (b) April–June; (c) July–September; (d) October–December

practice of predicting wet deposition from the monitoring data alone by using IDW, a significant reduction in mean-squared error, calculated over a set of validation sites, has been achieved. Inclusion of the significant covariate precipitation improves the predictive ability of our model, and these predictions can be expected to be better than the predictions that are based on the IDW method since that ignores the significant covariate.

The model was initially developed for sulphate deposition, but its success led us to consider nitrate deposition as well. The performance of the model for both sulphate and nitrate deposition encourages its application to other constituents of wet deposition.

Fig. 15. Maps showing the lengths of the 95% credible intervals for the nitrate predictions on four quarters: (a) January–March; (b) April–June; (c) July–September; (d) October–December

It is also of interest to estimate dry deposition, which is defined as the exchange of gases, aerosols and particles between the atmosphere and Earth's surface. Future analyses will focus on predicting total (wet plus dry) sulphur and nitrogen deposition. Using the total predictive surface it will be possible to estimate deposition 'loadings' as the integrated volume of total deposition over ecological regions of interest. For this, a new model for dry deposition must be developed. If successful, this effort will lead to the first ever estimation of total deposition loading, which is perhaps the most critical quantity for ecological assessments. Future work will also address trends in deposition to assess whether regulation has been successful.

Acknowledgements

The US Environmental Protection Agency's Office of Research and Development partially collaborated in the research that is described here. Although it has been reviewed by the Environmental Protection Agency and approved for publication, it does not necessarily reflect the Agency's policies or views. The authors thank Gary Lear and Norm Possiel of the US Environmental Protection Agency for providing the monitoring data and CMAQ output.

Appendix A: Distributions for Gibbs sampling

A.1. Handling of the missing values

Note that the transformation equation (3) does not define a unique value of $Y(\mathbf{s}_i, t)$ and, in addition, there will be missing values corresponding to the missing values in $Z(\mathbf{s}_i, t)$. Any missing value of $Y^*(\mathbf{s}_i, t)$ is sampled from the model value $N\{\vartheta(\mathbf{s}_i, t), \sigma_\varepsilon^2\}$ for $i = 1, \ldots, n$ and $t = 1, \ldots, T$.

The sampling of the missing $U^*(\mathbf{s}_i, t)$ for the precipitation process is a little more involved. The sampling of the missing values must be done by using model (6) conditionally on all the parameters. Since this model is a spatial model we must use the conditional distribution of $U^*(\mathbf{s}_i, t)$ given all the $U(\mathbf{s}_j, t)$ values for $j = 1, \ldots, n$ and $j \neq i$. This conditional distribution is obtained by using the covariance matrix Σ_δ of $\boldsymbol{\delta}_t$ and has been omitted for brevity.

Similarly, equation (4) does not define unique values of $X(A_j, t)$ when $Q(A_j, t) = 0$. Those values, which are denoted by $X^*(A_j, t)$, are sampled by using model (8); $X^*(A_j, t)$ is sampled from $N\{\gamma_0 + \gamma_1 \tilde{v}(A_j, t), \sigma_\psi^2\}$.

A.2. Conditional posterior distributions of $\boldsymbol{\theta}$

Straightforward calculation yields the following complete conditional distributions:

$$\frac{1}{\sigma_\varepsilon^2} \sim G\left\{\frac{nT}{2} + \nu, \lambda + \frac{1}{2}\sum_{t=1}^{T}(\mathbf{y}_t - \vartheta_t)'(\mathbf{y}_t - \vartheta_t)\right\},$$

$$\frac{1}{\sigma_b^2} \sim G\left(\frac{n}{2} + \nu, \lambda + \frac{1}{2}\mathbf{b}' S_b^{-1}\mathbf{b}\right),$$

$$\frac{1}{\sigma_\eta^2} \sim G\left(\frac{nT}{2} + \nu, \lambda + \frac{1}{2}\sum_{t=1}^{T}\boldsymbol{\eta}_t' S_\eta^{-1}\boldsymbol{\eta}_t\right),$$

$$\frac{1}{\sigma_\delta^2} \sim G\left\{\frac{nT}{2} + \nu, \lambda + \frac{1}{2}\sum_{t=1}^{T}(\mathbf{u}_t - \alpha_0\mathbf{1} - \alpha_1\mathbf{v}_t)' S_\delta^{-1}(\mathbf{u}_t - \alpha_0\mathbf{1} - \alpha_1\mathbf{v}_t)\right\},$$

$$\frac{1}{\sigma_\psi^2} \sim G\left\{\frac{JT}{2} + \nu, \lambda + \frac{1}{2}\sum_{t=1}^{T}(\mathbf{x}_t - \gamma_0\mathbf{1} - \gamma_1\tilde{\mathbf{v}}_t)'(\mathbf{x}_t - \gamma_0\mathbf{1} - \gamma_1\tilde{\mathbf{v}}_t)\right\},$$

$$\frac{1}{\sigma_v^2} \sim G\left\{\frac{nT}{2} + \nu, \lambda + \frac{1}{2}\sum_{t=1}^{T}(\mathbf{v}_t - \tilde{\mathbf{v}}_t^{(1)})'(\mathbf{v}_t - \tilde{\mathbf{v}}_t^{(1)})\right\},$$

$$\frac{1}{\sigma_\zeta^2} \sim G\left[\frac{JT}{2} + \nu, \lambda + \frac{1}{2}\sum_{t=1}^{T}\sum_{j=1}^{J} m_j\{\zeta(A_j, t) - \bar{\zeta}(A_j, t)\}^2\right]$$

where $\bar{\zeta}(A_j, t) = \Sigma_{i=1}^{J} h_{ji}\, \zeta(A_i, t)$.

Let $\boldsymbol{\beta} = (\beta_0, \beta_1, \beta_2)$ and $G_t = (\mathbf{1}, \mathbf{u}_t, \mathbf{v}_t)$ so that G_t is an $n \times 3$ matrix. The full conditional distribution of $\boldsymbol{\beta}$ is $N(\Lambda\boldsymbol{\chi}, \Lambda)$ where

$$\Lambda^{-1} = \frac{1}{\sigma_\varepsilon^2}\sum_{t=1}^{T} G_t' G_t + 10^{-3} I_3,$$

$$\boldsymbol{\chi} = \frac{1}{\sigma_\varepsilon^2}\sum_{t=1}^{T} G_t'(\mathbf{y}_t - b_0\mathbf{x}_t + X_t\mathbf{b} + \boldsymbol{\eta}_t).$$

The full conditional distribution of b_0 is $N(\Lambda\chi, \Lambda)$ where

$$\Lambda^{-1} = \frac{1}{\sigma_\varepsilon^2}\sum_{t=1}^{T}\mathbf{x}_t'\mathbf{x}_t + 10^{-3},$$

$$\chi = \frac{1}{\sigma_\varepsilon^2}\sum_{t=1}^{T}\mathbf{x}_t'(\mathbf{y}_t - \beta_0\mathbf{1} - \beta_1\mathbf{u}_t - \beta_2\mathbf{v}_t - X_t\mathbf{b} - \boldsymbol{\eta}_t).$$

The full conditional distribution of $\mathbf{b}$ is $N(\Lambda\boldsymbol{\chi}, \Lambda)$ where

$$\Lambda^{-1} = \frac{1}{\sigma_\varepsilon^2}\sum_{t=1}^{T}X_t'X_t + \Sigma_b^{-1},$$

$$\boldsymbol{\chi} = \frac{1}{\sigma_\varepsilon^2}\sum_{t=1}^{T}X_t'(\mathbf{y}_t - \beta_0\mathbf{1} - \beta_1\mathbf{u}_t - \beta_2\mathbf{v}_t - b_0\mathbf{x}_t - \boldsymbol{\eta}_t).$$

The full conditional distribution of $\boldsymbol{\eta}_t$ for $t = 1, \ldots, T$ is $N(\Lambda_t\boldsymbol{\chi}_t, \Lambda_t)$ where

$$\Lambda_t^{-1} = \frac{I_n}{\sigma_\varepsilon^2} + \Sigma_\eta^{-1},$$

$$\boldsymbol{\chi}_t = \frac{1}{\sigma_\varepsilon^2}(\mathbf{y}_t - \beta_0\mathbf{1} - \beta_1\mathbf{u}_t - \beta_2\mathbf{v}_t - b_0\mathbf{x}_t - X_t\mathbf{b}).$$

Let $G_t = (\mathbf{1}, \mathbf{v}_t)$ so that G_t is an $n \times 2$ matrix. The full conditional distribution of $\boldsymbol{\alpha} = (\alpha_0, \alpha_1)$ is $N(\Lambda\boldsymbol{\chi}, \Lambda)$ where

$$\Lambda^{-1} = \sum_{t=1}^{T}G_t'\Sigma_\delta^{-1}G_t + 10^{-3}I_2,$$

$$\boldsymbol{\chi} = \sum_{t=1}^{T}G_t'\Sigma_\delta^{-1}\mathbf{u}_t.$$

Let $G_t = (\mathbf{1}, \tilde{\mathbf{v}}_t)$ so that G_t is a $J \times 2$ matrix. The full conditional distribution of $\boldsymbol{\gamma} = (\gamma_0, \gamma_1)$ is $N(\Lambda\boldsymbol{\chi}, \Lambda)$ where

$$\Lambda^{-1} = \frac{1}{\sigma_\psi^2}\sum_{t=1}^{T}G_t'G_t + 10^{-3}I_2,$$

$$\boldsymbol{\chi} = \sum_{t=1}^{T}G_t'\mathbf{x}_t.$$

The full conditional distribution of ρ is $N(\Lambda\chi, \Lambda)$ where

$$\Lambda^{-1} = \frac{1}{\sigma_\zeta^2}\sum_{t=1}^{T}\sum_{j=1}^{J}m_j e_{j,t-1}^2 + 10^{-3},$$

$$\chi = \frac{1}{\sigma_\zeta^2}\sum_{t=1}^{T}\sum_{j=1}^{J}m_j e_{jt}e_{j,t-1}$$

where $e_{jt} = \tilde{v}(A_j, t) - \bar{v}(A_j, t)$ and $\bar{v}(A_j, t) = \Sigma_{i=1}^{J}h_{ji}\tilde{v}(A_i, t)$, restricted in the interval (0,1).

A.3. Conditional posterior distributions of $\mathbf{V}_t$

Owing to the missing and zero precipitation values the full conditional distribution of $\mathbf{V}_t$ will be in a restricted space. First, the unrestricted full conditional distribution of $\mathbf{v}_t$ is $N(\Lambda_t\boldsymbol{\chi}_t, \Lambda_t)$ where

$$\Lambda_t^{-1} = \beta_2^2\frac{I_n}{\sigma_\varepsilon^2} + \alpha_1^2\Sigma_\delta^{-1} + \frac{I_n}{\sigma_v^2},$$

$$\boldsymbol{\chi}_t = \frac{\beta_2}{\sigma_\varepsilon^2}\mathbf{a}_t + \alpha_1\Sigma_\delta^{-1}(\mathbf{u}_t - \alpha_0\mathbf{1}) + \frac{1}{\sigma_v^2}\tilde{\mathbf{v}}_t^{(1)},$$

where $\mathbf{a}_t = \mathbf{y}_t - \beta_0\mathbf{1} - \beta_1\mathbf{u}_t - b_0\mathbf{x}_t - X_t\mathbf{b} - \boldsymbol{\eta}_t$. From this n-dimensional joint distribution we obtain the conditional distribution $V(\mathbf{s}_i, t) \sim N(\mu_{it}, \Xi_{it})$, say. If the precipitation value $p(\mathbf{s}_i, t)$ is missing then there will be no constraint on $V(\mathbf{s}_i, t)$ and we sample $V(\mathbf{s}_i, t)$ unrestricted from $N(\mu_{it}, \Xi_{it})$. If, however, the observed precipitation value is zero, $p(\mathbf{s}_i, t) = 0$, we must sample $V(\mathbf{s}_i, t)$ to be negative, i.e. we sample from $N(\mu_{it}, \Xi_{it})\, I\{V(\mathbf{s}_i, t) < 0\}$. Corresponding to non-zero precipitation value $p(\mathbf{s}_i, t) > 0$ we sample $V(\mathbf{s}_i, t)$ from $N(\mu_{it}, \Xi_{it})\, I\{V(\mathbf{s}_i, t) > 0\}$.

A.4. Conditional posterior distributions of $\tilde{\mathbf{V}}_t$

The full conditional distribution of $\tilde{\mathbf{V}}_t = (\tilde{\mathbf{V}}_t^{(1)}, \tilde{\mathbf{V}}_t^{(2)})$ for any t is $N(\Lambda_t\boldsymbol{\chi}_t, \Lambda_t)$ where

$$\Lambda_t^{-1} = \begin{pmatrix} I_n/\sigma_v^2 & 0 \\ 0 & 0 \end{pmatrix} + \gamma_1^2\frac{I_J}{\sigma_\psi^2} + \{1 + I(t<T)\rho^2\}D^{-1}(I - H),$$

$$\boldsymbol{\chi}_t = \begin{pmatrix} (1/\sigma_v^2)\mathbf{v}_t \\ 0 \end{pmatrix} + \frac{\gamma_1}{\sigma_\psi^2}(\mathbf{x}_t - \gamma_0\mathbf{1}) + \rho D^{-1}(I - H)\{\tilde{\mathbf{v}}_{t-1} + I(t<T)\tilde{\mathbf{v}}_{t+1}\}$$

where $I(t<T) = 1$ if $t = 1, \ldots, T-1$ and $I(t<T) = 0$ otherwise.

This full conditional distribution is a J-variate normal distribution where J is possibly very high (33 390 in our example) and simultaneous update is computationally prohibitive. In addition, we need to incorporate the constraints that are implied by the first-stage likelihood specification (5). The partition of $\tilde{\mathbf{V}}_t$, however, suggests an immediate univariate sampling scheme as follows.

The conditional prior distribution for $\tilde{V}(A_j, t)$, for each j and t, from the vectorized specification (12), as calculated above, is given by $N(\xi_{jt}, \omega_{jt}^2)$ where

$$\omega_{jt}^2 = \sigma_\zeta^2\frac{1}{m_j\{1 + I(t<T)\rho^2\}},$$

$$\xi_{jt} = r_{jt} + \sum_{i=1}^{J} h_{ji}\{\tilde{v}(A_i, t) - r_{it}\}$$

where r_{jt} is the jth element of

$$\mathbf{r}_t = \frac{\rho}{1 + I(t<T)\rho^2}\{\tilde{\mathbf{v}}_{t-1} + I(t<T)\tilde{\mathbf{v}}_{t+1}\}.$$

The form of the likelihood contribution for $\tilde{V}(A_j, t)$ will depend on whether $\tilde{V}(A_j, t)$ is one of $\tilde{\mathbf{V}}_t^{(1)}$ or one of $\tilde{\mathbf{V}}_t^{(2)}$. For each component $\tilde{V}(A_j, t)$ of $\tilde{\mathbf{V}}_t^{(1)}$ we extract the full conditional distribution to be viewed as the likelihood contribution from the joint distribution $N(\Lambda_{(1),t}\boldsymbol{\chi}_{(1),t}, \Lambda_{(1),t})$ where

$$\Lambda_{(1),t}^{-1} = \frac{I_n}{\sigma_v^2} + \gamma_1^2\frac{I_n}{\sigma_\psi^2},$$

$$\boldsymbol{\chi}_{(1),t} = \frac{1}{\sigma_v^2}\mathbf{v}_t + \frac{\gamma_1}{\sigma_\psi^2}(\mathbf{x}_t - \gamma_0\mathbf{1}).$$

This conditional likelihood contribution is given by $N(\mu_{jt}, \Xi^2)$ where

$$\mu_{jt} = \Xi^2\left[\frac{\tilde{v}(A_j, t)}{\sigma_v^2} + \frac{\gamma_1\{x(A_j, t) - \gamma_0\}}{\sigma_\psi^2}\right],$$

$$\Xi^2 = \frac{1}{1/\sigma_v^2 + \gamma_1^2/\sigma_\psi^2}.$$

For each component $\tilde{V}(A_j, t)$ of $\tilde{\mathbf{V}}_t^{(2)}$ the likelihood contribution is also denoted by the normal distribution $N(\mu_{jt}, \Xi^2)$ where

$$\mu_{jt} = \frac{x(A_j, t) - \gamma_0}{\gamma_1},$$

$$\Xi^2 = \sigma_\psi^2/\gamma_1^2.$$

Now the unconstrained full conditional distribution of $\tilde{V}(A_j, t)$, according to the second-stage likelihood and prior specification, is obtained by combining the likelihood contribution $N(\mu_{jt}, \Xi^2)$ and the prior conditional distribution $N(\xi_{jt}, \omega_{jt}^2)$ and is given by $N(\Lambda_{jt}\chi_{jt}, \Lambda_{jt})$ where

$$\Lambda_{jt}^{-1} = \Xi^{-2} + \omega_{jt}^{-2},$$
$$\chi_{jt} = \Xi^{-2}\mu_{jt} + \omega_{jt}^{-2}\xi_{jt}.$$

To respect the constraints that are implied by the first-stage specification we simulate the $\tilde{V}(A_j, t)$ to be positive if $X(A_j, t) > 0$ and negative otherwise.

References

Banerjee, S., Carlin, B. P. and Gelfand, A. E. (2004) *Hierarchical Modeling and Analysis for Spatial Data*. Boca Raton: Chapman and Hall–CRC.

Bilonick, R. A. (1985) The space-time distribution of sulfate deposition in the northeastern United States. *Atmos. Environ.*, **19**, 1829–1845.

Brook, J. R., Samson, P. J. and Sillman, S. (1995) Aggregation of selected three-day periods to estimate annual and seasonal wet deposition totals for sulfate, nitrate, and acidity: part I, a synoptic and chemical climatology for eastern North America. *J. Appl. Meteorol.*, **34**, 297–325.

Brown, P. J., Le, N. D. and Zidek, J. V. (1994) Multivariate spatial interpolation and exposure to air pollutants. *Can. J. Statist.*, **22**, 489–510.

Carroll, R. J., Chen, R., George, E. I., Li, T. H., Newton, H. J., Schmiediche, H. and Wang, N. (1997) Ozone exposure and population density in Harris County, Texas. *J. Am. Statist. Ass.*, **92**, 392–404.

Fuentes, M. and Raftery, A. (2005) Model evaluation and spatial interpolation by Bayesian combination of observations with outputs from numerical models. *Biometrics*, **61**, 36–45.

Gelfand, A. E. and Ghosh, S. K. (1998) Model choice: a minimum posterior predictive loss approach. *Biometrika*, **85**, 1–11.

Goulard, M. and Voltz, M. (1992) Linear coregionalization model: tools for estimation and choice of multivariate variograms. *Math. Geol.*, **24**, 269–286.

Gotway, C. A. and Young, L. J. (2002) Combining incompatible spatial data. *J. Am. Statist. Ass.*, **97**, 632–648.

Grimm, J. W. and Lynch, J. A. (2004) Enhanced wet deposition estimates using modeled precipitation inputs. *Environ. Monit. Assessmnt*, **90**, 243–268.

Haas, T. C. (1990a) Lognormal and moving window methods of estimating acid deposition. *J. Am. Statist. Ass.*, **85**, 950–963.

Haas, T. C. (1990b) Kriging and automated variogram modeling within a moving window. *Atmos. Environ.* A, **24**, 1759–1769.

Haas, T. C. (1995) Local prediction of a spatio-temporal process with an application to wet sulfate deposition. *J. Am. Statist. Ass.*, **90**, 1189–1199.

Haas, T. C. (1996) Multivariate spatial prediction in the presence of non-linear trend and covariance non-stationarity. *Environmetrics*, **7**, 145–165.

Huerta, G., Sansó, B. and Stroud, J. R. (2004) A spatiotemporal model for Mexico City ozone levels. *Appl. Statist.*, **53**, 231–248.

Le, N. and Zidek, J. (1992) Interpolation with uncertain spatial covariances: a Bayesian alternative to kriging. *J. Multiv. Anal.*, **43**, 351–374.

Oehlert, G. W. (1993) Regional trends in sulfate wet deposition. *J. Am. Statist. Ass.*, **88**, 390–399.

Rappold, A. G., Gelfand, A. E. and Holland, D. M. (2008) Modelling mercury deposition through latent space–time processes. *Appl. Statist.*, **57**, 187–205.

Sahu, S. K., Gelfand, A. E. and Holland, D. M. (2006) Spatio-temporal modeling of fine particulate matter. *J. Agric. Biol. Environ. Statist.*, **11**, 61–86.

Sahu, S. K., Gelfand, A. E. and Holland, D. M. (2007) High resolution space-time ozone modeling for assessing trends. *J. Am. Statist. Ass.*, **102**, 1221–1234.

Sahu, S. K. and Mardia, K. V. (2005) A Bayesian kriged–Kalman model for short-term forecasting of air pollution levels. *Appl. Statist.*, **54**, 223–244.

Sahu, S. K., Yip, S. and Holland, D. M. (2009) Improved space-time forecasting of next day ozone concentrations in the eastern U.S. *Atmos. Environ.*, **43**, 494–501.

Stein, M. L. (1999) *Interpolation of Spatial Data: Some Theory for Kriging*. New York: Springer.

Wikle, C. K. (2003) Hierarchical models in environmental science. *Int. Statist. Rev.*, **71**, 181–199.

Zhang, H. (2004) Inconsistent estimation and asymptotically equal interpolations in model-based geostatistics. *J. Am. Statist. Ass.*, **99**, 250–261.